Lifetimes of $N=Z$ nuclei ^{66}As and ^{70}Br

R. H. Burch Jr., C. A. Gagliardi, and R. E. Tribble
Cyclotron Institute, Texas A&M University, College Station, Texas 77843
(Received 5 May 1988)

We have utilized a rapid-transport target system together with a β-ray range telescope to remeasure the half-lives of the $N=Z$, odd-odd nuclei ^{66}As and ^{70}Br. We find they are 95.77±0.28 ms and 78.54±0.59 ms, respectively. The ^{66}As result is in good agreement with the previous study, while the ^{70}Br measurement differs somewhat from the previous result.

I. INTRODUCTION

The best known element of the Kobayashi-Maskawa quark mixing matrix is U_{ud}. It is determined[1,2] by comparing the vector coupling constant G_V of nuclear beta decay to the Fermi coupling constant G_F determined from muon decay, after correcting G_V for "inner" radiative effects[1] that depend upon the assumed substructure of the nucleon. An accurate determination of U_{ud} is necessary to test the unitarity of the Kobayashi-Maskawa matrix, a measure of the number of generations. The ft values of the $0^+\rightarrow 0^+$ superallowed Fermi beta decays provide the most sensitive measurement of G_V. Eight cases, from ^{14}O to ^{54}Co, are known to $<0.2\%$. Before G_V may be extracted from these measured ft values, they must be corrected for "outer" radiative and Coulomb effects. The outer radiative corrections depend on the nuclear charge and size and on the total energy released in the decay. They are believed to be known[2,3] to $<0.1\%$. The Coulomb corrections,[4,5] which depend upon the detailed structures of the parent and daughter nuclei, are considerably less certain. In general, they tend to increase approximately as Z^2, so it is of interest to measure heavier cases to test the accuracy of these calculations.

The highest Z $0^+\rightarrow 0^+$ Fermi transition whose ft value has been measured to date[6] is ^{62}Ga, which is currently known to 1.5%. This uncertainty is dominated by our knowledge of the ^{62}Ga endpoint energy, as the half-life is known to 0.2%. By contrast, the half-lives of ^{66}As and ^{70}Br, the next two nuclei with $0^+\rightarrow 0^+$ Fermi beta decays, have only been determined[7] to 0.4% and 1.0%, respectively, and their endpoint energies have not yet been measured. As a first step in an effort to extend our knowledge of superallowed Fermi decays to higher Z systems, we have remeasured the half lives of ^{66}As and ^{70}Br, using a detection system that is subject to different systematic effects from those associated with the previous experiment. While our ^{66}As half-life agrees with the previous measurement, our ^{70}Br half-life determination differs somewhat from the previous result. In Sec. II we describe the detector system developed for this measurement. In Sec. III we discuss the data analysis and results. In Sec. IV we provide some conclusions.

II. EXPERIMENTAL PROCEDURES

^{66}As was produced with the reaction ^{58}Ni(^{10}B,2n)^{66}As, using 29.5 and 30.5 MeV $^{10}B^{2+}$ beams from the Texas A&M University 224-cm Cyclotron. ^{70}Br was produced with the reaction ^{58}Ni(^{14}N,2n)^{70}Br, using a 42.5 MeV $^{14}N^{3+}$ beam. Figure 1 shows a schematic layout of the beamline and target chamber, including the β-ray detector and shielding. The beams passed through movable X-Y collimator slits located 5.3 m before the target. These slits defined the beam size at the target and ensured that no beam passed around a piston-driven beam shutter, the forward Faraday cup (FC_f), when it was closed. FC_f was used to chop the beam on target mechanically. We observed <2 pA on target with FC_f shut when the slits were opened to 2×2 cm^2. FC_f also served as the primary aid used in keeping the cyclotron beams tuned, since the beam remained on FC_f over 90% of the time. Typical beam currents on target were 600 nA, with 80% transmission between FC_f and the target.

To reduce the buildup of long-lived activities, a rapid-transport target system was employed. Twenty equally spaced targets, each consisting of 5.0 mg/cm^2 of 99.89% enriched ^{58}Ni, were mounted on a 15.2-cm diameter Al wheel. A Ta collimator placed at the entrance to the target chamber prevented the beam from hitting the target wheel during the irradiation periods. A Slo-Syn stepping motor (M series), coupled to the target wheel via a Ferrofluidic feedthrough, rotated it on demand. A preset

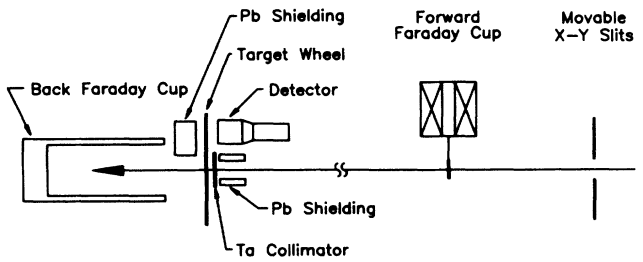

FIG. 1. A schematic diagram of the beamline and target chamber, showing the relative locations of the target wheel, the detector telescope, and the detector shielding.

indexer with an antibacklash circuit drove the stepping motor. After each irradiation, the target wheel was rotated 54° (±0.083% noncumulative), which moved the activated target from the beam axis to a location in front of the β-detector telescope. Rotation times were <50 ms. This rapid-transport target system reduced the yield of the long-lived activities by a factor of ≈ 20 compared to previous measurements, while maintaining the yield of the short-lived activities of interest.

The β-ray detector telescope, which is shown in Fig. 2, was located 54° clockwise from the target in a well-shielded environment. The Ta beam collimator was shielded from the telescope by 3 mm of Pb, while the beam stop was shielded from the detector by 5.2 cm of Pb. The telescope consisted of four 1.02-mm thick BC 412 scintillator disks coupled to 3.2-mm thick Lucite light guides with optical cement. The light guides connected the scintillator disks to RCA 8575 photomultiplier tubes (PMT's). The detector elements were positioned for maximum solid angle while reserving the option of inserting Lucite absorbers between them. A 1.6-mm thick Lucite disk was permanently located in front of the first detector element to range-out low-energy β rays and soft photons. The light guides also acted as absorbers. High energy β rays were identified by fourfold coincidences among the detector elements. Low-energy β rays were discriminated against by their range in the detector telescope. The effective energy threshold was adjusted by varying the amount of additional absorber material present. Typically, it was ≈ 4.5 MeV.

This β-ray detector telescope provided several advantages over a single plastic scintillator. It was immune to the pile-up effects inherent in pulse-height discrimination because the intense, low-energy activities were ranged out before they reached the back detectors. Discriminator shifts that would result in a change in the energy threshold of a single detector could not affect our system unless they were severe, since the thresholds were set to $\approx \frac{1}{2}$ minimum ionizing. Finally, the transparency of our detector to photons minimized the probability of misidentifying β-γ cascades as high energy positrons. These advantages resulted in a substantial improvement in the overall S/N ratio.

A fifth detector element, a 6.4-mm thick plastic scintillator, was placed above the telescope to serve as a veto counter when it became apparent that nontarget related backgrounds were dominated by cosmic-ray air showers. A 1.27-cm thick Al plate shielded the veto scintillator from the telescope to ensure that no β rays of interest would produce a veto signal.

The anode outputs from the PMT's were fed into constant fraction discriminators (CFD's). The timing of the CFD signals was adjusted using ^{58}Cu β rays following the reaction ^{58}Ni$(p,n)^{58}$Cu. The 20-nsec wide CFD outputs from the first, second, and third detector elements were required to be in coincidence with a 10-nsec wide CFD output from the fourth detector element and in anticoincidence with the veto counter. Events which passed this trigger logic were routed to the multichannel scaling input of a Nucleus Personal Computer Analyzer. The sequencing of the target transport and irradiation systems was controlled by a master clock which triggered a series of gate and delay generators. Figure 3 shows a typical timing diagram for the measurements.

III. DATA ANALYSIS AND RESULTS

The major problem in determining the half-lives of ^{66}As and ^{70}Br from the data was to find appropriate fitting functions that treated the contaminants properly. Preliminary studies determined that ^{20}Na, produced in the ^{12}C(^{10}B,2n)^{20}Na reaction off of carbon contamination on the surface of the Ni targets, was a serious background problem in the ^{66}As data. This work also indicated that long-lived activities produced in the target would create a nearly constant background through β-γ coincidences in the detector telescope. The experimental setup described above was designed to reduce carbon contamination, by minimizing the amount of integrated

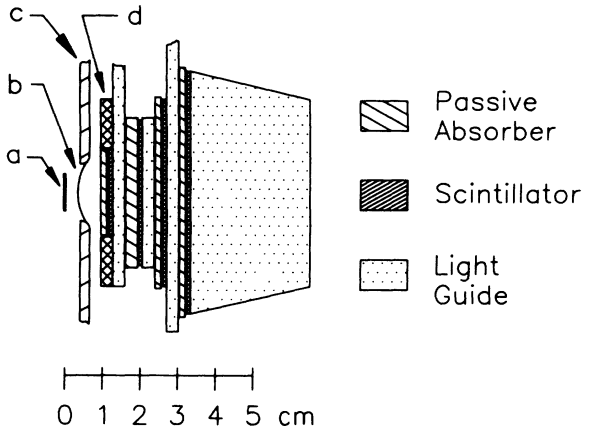

FIG. 2. The β-ray detector range telescope. The labeled items are (a) the target location, (b) the Mylar vacuum window, (c) the Al wall of the vacuum chamber, and (d) a Ta collimator to shield the telescope from the neighboring targets.

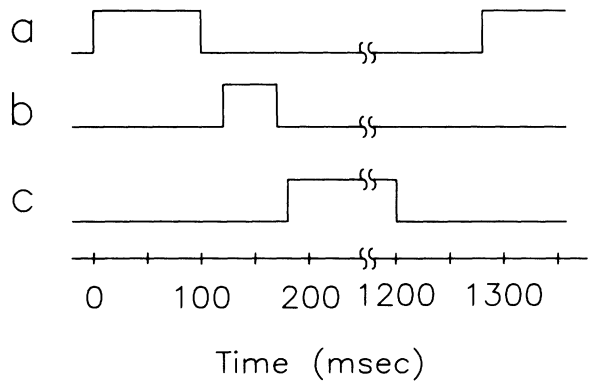

FIG. 3. A typical timing sequence for the experiment. (a) Represents the beam on target time. (b) Represents the target rotation time. (c) Represents the multiscale counting interval. The counting interval shown was used for the ^{70}Br measurements. For the ^{66}As measurements, the counting interval was twice as long, while all other time intervals were unchanged. The delay between (a) and (b) ensured that no beam struck the Al target wheel during rotation.

beam on an individual target, in addition to minimizing our sensitivity to long-lived backgrounds as discussed above.

In order to check for the possible presence of additional short-lived background activities, we used the code CASCADE (Ref. 8) to estimate the yield of isotopes, with half-lives less than a few seconds, that would be produced by compound nucleus evaporation off either ^{58}Ni or likely contaminants. In addition to ^{20}Na, the ^{10}B beam was predicted to produce ^{62}Ga, but with a yield that was less than 0.4% of the ^{66}As yield. Since the ^{62}Ga half-life is only $\approx$20 ms longer than the ^{66}As half-life, a background of this magnitude would change our fitted result by less than 0.08 ms. The only significant short-lived background associated with the ^{14}N beam at our beam energy was ^{24}Al, produced in the reaction ^{12}C(^{14}N,2n)^{24}Al. ^{24}Al is an extremely troublesome contaminant since it has a high-energy β decay from a metastable state with a half-life of $\approx$130 ms. This is sufficiently close to the ^{70}Br half-life that it would be virtually impossible to distinguish the two isotopes from our data. The ^{24}Al ground state has a half-life of $\approx$2 sec, which makes it difficult to separate its decay from the other long-lived activities that we produced.

To check these predictions, we bombarded a 3.4-mg/cm^2 thick natural C target with both ^{14}N and ^{10}B beams, using the same beam energies and experimental setup that were used for the half-life determinations. The irradiations were carried out with a single target placed on the target wheel, while the remaining 19 locations were left blank. The same timing sequence as for the ^{58}Ni irradiations was used, except that after multiscaling the activity from the C target, the target wheel was rapidly rotated 19 times to return the target to the beam. With the ^{10}B beam, we observed only ^{20}Na in the spectrum. With the ^{14}N beam, we observed a clear signature for the production of both ^{24}Al and ^{24}Al^m. We fit the ^{24}Al data with the four-parameter fitting function:

$$y(t_i)=a+b\exp[-(ln2)t_i/t_1] +c\exp[-(\ln2)t_i/t_2]\ , \tag{1}$$

where $y(t_i)$ is the predicted number of counts in the ith time bin, a represents a constant (long-lived) background, b and c represent the ^{24}Al^m and ^{24}Al yields, respectively, in the first time bin, and t_1 and t_2 are their half-lives. a, b, c, and t_1 were treated as free parameters, while t_2 was fixed at 2.066±0.010 sec.[9] We obtained a half-life of 132.7±4.1 ms for ^{24}Al^m, in excellent agreement with the accepted value[9] of 130±4 ms. We determined the total ^{24}Al yield and the ^{24}Al/^{24}Al^m ratio from this data.

Since different backgrounds were present in the two reactions, different fitting functions were employed for the ^{66}As and ^{70}Br spectra. For the ^{66}As data, the form of the fitting function was identical to that used for the ^{24}Al data, except t_1 represented the half-life of ^{66}As and t_2 was fixed at 446±3 ms; the half-life of ^{20}Na.[10] For the ^{70}Br data, we used the functional form

$$y(t_i)=a+b\exp[-(\ln2)t_i/t_1] +c\exp[-\ln2t_i/t_2] +d\exp[-(\ln2)t_i/t_3]\ , \tag{2}$$

where $y(t_i)$ and a are as defined above. b, c, and d are the ^{70}Br, ^{24}Al^m, and ^{24}Al yields in the first time bin, while t_1, t_2, and t_3 are their respective half-lives. a, b, and t_1 were treated as free parameters. t_2 and t_3 were fixed at 131.3±2.8 ms, the weighted mean of our new ^{24}Al^m half-life measurement and the previous value, and 2.066±0.010 ms, while c and d were fixed as discussed below.

Three different χ^2 minimization fitting routines were used to provide an internal consistency check among the programs. All three routines agreed within the expected accuracies of the algorithms that they employed. The final results quoted below were obtained from the routine CURFIT.[11] The statistical uncertainties in the fits were estimated by extracting the curvature matrix from CURFIT and calculating the covariant matrix.

The use of χ^2 minimization required special treatment of the statistical uncertainties in the time spectra to obtain unbiased fits. Since the time spectra here obey Poisson statistics, one typically would take the uncertainty σ_i in a measured yield y_i to be $\sqrt{y_i}$. But in that case, a χ^2 minimization will systematically underestimate the data.[11] This problem is particularly important when fitting data with relatively few counts per channel, as is the case for the late channels of our multiscaled spectra. To avoid this problem, we obtained initial estimates of the uncertainties σ_i from binominally weighted five-channel averages of our spectra. Then, after finding an initial "best-fit," we reevaluated our uncertainties according to $\sigma_i=[y_{\rm fit}(t_i)]^{1/2}$. We iterated this procedure until it converged, which typically required four passes. It is important to note that our choice for the initial estimates of σ_i did not change the ultimate fits, but merely accelerated the convergence process.

Table I gives the results for the fits to the ^{66}As data. In addition to the four-parameter fits described above, the table shows the results of a three-parameter fit, in which the ^{20}Na amplitude was set to zero. Results for the data taken at both beam energies are included, as well as the results for the combined data set. It is clear from the χ^2 that the three-parameter fit is poor. In Fig. 4 we show the fit to the combined data set along with residual plots for both the three- and four-parameter cases. The residuals are defined as

$$R_i=\frac{y(t_i)-y_i}{\sigma_i}\ , \tag{3}$$

where $y(t_i)$ and y_i are the fitted and measured yields in the ith time bin and σ_i is the uncertainty in that bin. The residual plot for the three-parameter fit clearly indicates the need for an additional term in the fitting function by its systematic deviation from the data.

The ^{24}Al backgrounds made the ^{70}Br data more difficult to fit than the ^{66}As data. As noted above, the

TABLE I. Results of the ^{66}As half-life fits. The parameters are defined in Eq. (1).

	a	b	t_1	c	χ^2_ν
30.5 MeV data	25.87±0.98	11 747±40	95.81±0.34	69.4±7.7	1.06
29.5 MeV data	11.60±0.66	5314±27	95.69±0.50	29.7±5.1	1.03
Combined data:					
four-parameter fit	37.5±1.2	17 061±49	95.77±0.28	99.3±9.2	1.02
three-parameter fit	49.0±0.59	16 964±47	97.83±0.21	0.0	1.47

half-life of ^{24}Al^m is so close to that of ^{70}Br that it is difficult to separate the two species, while the half-life of ^{24}Al is sufficiently long that it is difficult to separate from the constant background that underlies the ^{70}Br data with only a 1 sec long counting period. Therefore, we estimated the c and d parameters in Eq. (2) from the results of our C target irradiations and our ^{66}As fits. We corrected the ^{24}Al/^{24}Al^m ratio for the difference in the timing sequence between the single C target and the multiple ^{58}Ni targets. Otherwise, it was the same for the ^{70}Br data since we used the same absorbers in the detector telescope and the same discriminator thresholds. The only missing parameter in the equation is the amount of ^{24}Al in the first time bin. From the C data, we know the yields of ^{24}Al and ^{20}Na. We estimated the average C thickness on the ^{58}Ni targets during the ^{10}B irradiation from the ^{20}Na yield in the ^{66}As data. These results show evidence for carbon build-up during the ^{10}B irradiation, with an average of 3.6±1.2 μg/cm^2 present when the ^{10}B irradiation began. The ^{10}B beam was run after the ^{14}N beam, so this represents an upper limit on the C thickness present during the ^{14}N runs. Since we do not know the initial C concentration, we have chosen to be conservative and estimate the average thickness to be 2.2±1.4 μg/cm^2. We combined these results to calculate the c and d coefficients in Eq. (2), and then fixed them. The resulting three-parameter fit (a, b, and t_1) gives the lifetime quoted in Table II. In addition to the statistical error quoted in the table, there is a systematic error of 0.37 ms due to the uncertainty in the C thickness. The fit and its associated residual plot is shown in Fig. 5. The table also shows the results of a three-parameter fit with the c and d coefficients set to zero. It is virtually indistinguishable from the fit that includes the ^{24}Al background activity. As a further check, we successively removed the first

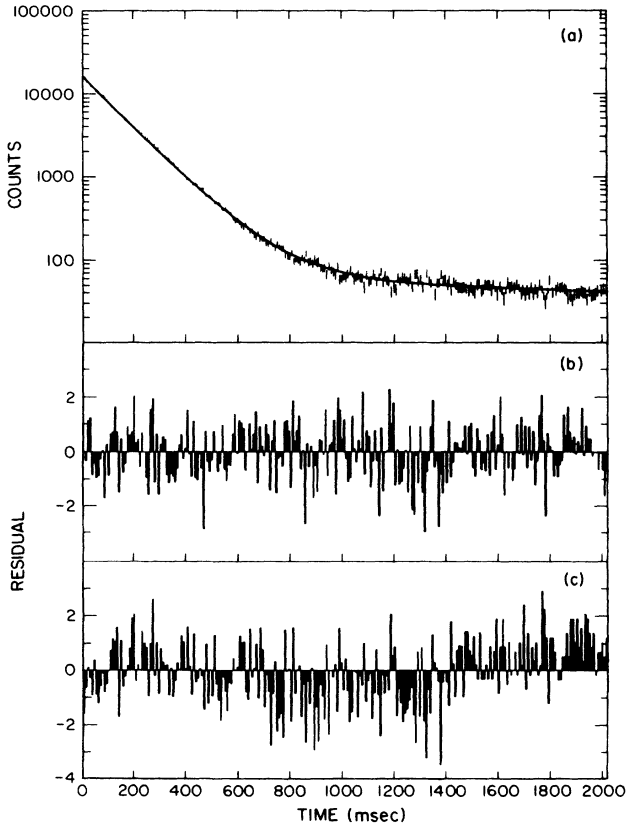

FIG. 4. Panel (a) shows the total ^{66}As half-life data, together with the four-parameter fit, including the ^{20}Na background activity, discussed in the text. Panel (b) shows the residual plot for the four-parameter fit. Panel (c) shows the residual plot for the three-parameter fit which excluded the ^{20}Na background contribution.

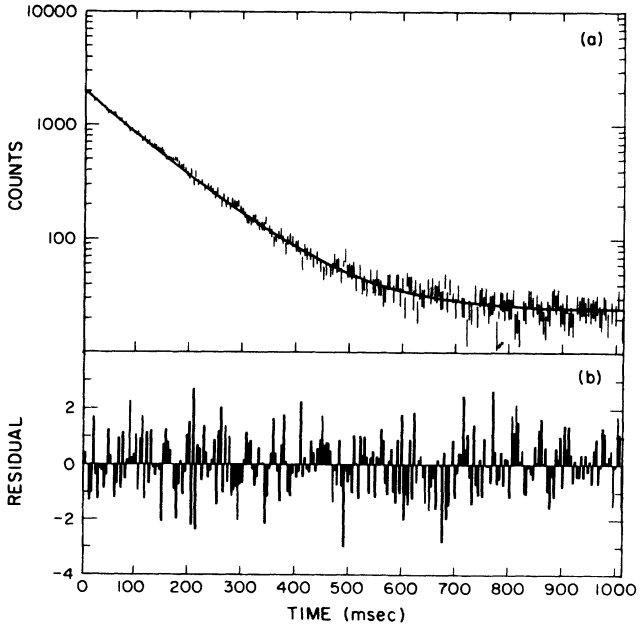

FIG. 5. Panel (a) shows the ^{70}Br half-life data, together with the three-parameter fit that explicitly included the ^{24}Al contributions, as discussed in the text. Panel (b) shows the residual plot associated with the fit.

TABLE II. Results of the ^{70}Br half-life fits. The parameters are defined in Eq. (2). The uncertainties quoted are purely statistical. There is an additional systematic error due to the uncertainty in the thickness of the C contamination.

	a	b	t_1	χ^2_ν
Including ^{24}Al background	23.92±0.50	1994±13	78.54±0.46	1.07
Neglecting ^{24}Al background	24.36±0.51	2010±13	79.10±0.46	1.08

several time bins from our data sets and recalculated the half-lives. No systematic trend was observed for either nucleus.

IV. CONCLUSIONS

We find that the half-lives of ^{66}As and ^{70}Br are 95.77±0.28 ms and 78.54±0.59 ms, respectively. The ^{66}As value is in good agreement with the previous result,[7] 95.78±0.39 ms, while the ^{70}Br value differs from the previous measurement of 80.2±0.8 ms. The previous experiment produced ^{70}Br using a 44 MeV ^{14}N beam. Our ^{58}Ni + ^{14}N CASCADE calculations predict that, at 42.5 MeV, this reaction should only produce ≈0.1% as much ^{66}As as ^{70}Br. By contrast, this ratio is predicted to be 8% for a 44 MeV ^{14}N beam. Thus, it is possible that the previous ^{70}Br experiment was contaminated with ^{66}As and ^{24}Al, leading to an anomalously long half-life. It is interesting to note that the ^{70}Br half-life that we obtain when we neglect the ^{24}Al contamination agrees with the previous measurement. However, the results of our C and ^{66}As studies clearly demonstrate that it is present, and therefore, it must be include in our fitting procedures.

Endpoint energy determinations are needed, in addition to the half-lives reported here, before the ft values of the ^{66}As and ^{70}Br β decays can be compared to the lower Z $0^+ \rightarrow 0^+$ Fermi transitions. It is unlikely that either of these nuclei could be produced in an exotic nuclear reaction, such as ^{64}Zn(^{10}B,^{8}He)^{66}As, with sufficient intensity to determine its mass accurately with a Q-value measurement. These endpoint energies will need to be determined by direct observation of the associated β rays. Endpoint energy determinations are far more sensitive to the presence of high-energy backgrounds, like ^{20}Na and ^{24}Al^m, than half-life measurements are. At present, we are pursuing efforts to produce purer samples of these nuclei, in order to proceed with the necessary mass measurements.

This work was supported in part by the U.S. Department of Energy and the Robert A. Welch Foundation.

[1]W. A. Marciano and A. Sirlin, Phys. Rev. Lett. **56**, 22 (1986).
[2]A. Sirlin and R. Zucchini, Phys. Rev. Lett. **57**, 1994 (1986).
[3]A. Sirlin, Phys. Rev. **164**, 1767 (1967).
[4]I. S. Towner, J. C. Hardy, and M. Harvey, Nucl. Phys. **A284**, 269 (1977).
[5]W. E. Ormand and B. A. Brown, Nucl. Phys. **A440**, 274 (1985).
[6]C. N. Davids, C. A. Gagliardi, M. J. Murphy, and E. B. Norman, Phys. Rev. C **19**, 1463 (1979).
[7]D. E. Alburger, Phys. Rev. C **18**, 1875 (1978).
[8]F. Puhlhofer, Nucl. Phys. **A280**, 267 (1977).
[9]P. M. Endt and C. Van der Leun, Nucl. Phys. **A310**, 1 (1978).
[10]F. Ajzenberg-Selove, Nucl. Phys. **A392**, 1 (1983).
[11]P. R. Bevington, *Data Reduction and Error Analysis for the Physical Sciences* (McGraw-Hill, New York, 1969).